Hindawi
Advances in Civil Engineering
Volume 2019, Article ID 1365759, 13 pages
https://doi.org/10.1155/2019/1365759

Research Article

A Method for Cavity Scale Estimation Based on Ground-Penetrating Radar (GPR) Explorations: An Experimental Study

Jeong-Jun Park,[1] **Yoonseok Chung**,[2] **and Gigwon Hong**[3]

[1]*Incheon Disaster Prevention Research Center, Incheon National University, 119 Academy-ro, Yeonsu-gu, Incheon 22012, Republic of Korea*
[2]*Korea Conformity Laboratories, 199 Gasan digital1-ro, Geumcheon-gu, Seoul 08503, Republic of Korea*
[3]*Institute of Technology Research and Development, Korea Engineering & Construction, 3-16, Jungdae-ro 25-gil, Songpa-gu, Seoul 05661, Republic of Korea*

Correspondence should be addressed to Gigwon Hong; gigwon_hong@kecgroup.kr

Received 27 September 2019; Accepted 22 November 2019; Published 27 December 2019

Guest Editor: Young-Suk Song

This study described the results of experiments comparing the cavity scales obtained from the GPR exploration with the direct excavation of the identified cavity scales. The first experiment was carried out on the actual roadway, and the additional experiment was carried out on the mock-up site to prevent the cavity collapse under the ground. It was confirmed that the soil depth of the predicted cavity and the identified cavity was similar, but the predicted cavity scales by GPR exploration overestimated the longitudinal and cross-sectional widths compared with the identified cavity scales. Based on the correlation between the cavity scales predicted by GPR exploration and the cavity scales identified in the mock-up test, an empirical formula for estimating the cavity scales was proposed.

1. Introduction

In Seoul, Korea, there have been large and small ground subsidence since 2014, which have become a social issue. Most ground subsidence occurred in the pavement of urban areas, and the main causes are supposed to be the improper construction of water supply pipes, sewers, gas pipes, and subways under the pavement. The analysis of the location of the roadway cavity that occurred in the past five years in Seoul revealed that 81% of cavities occurred at a depth less than 0.8 m, 17% of cavities occurred at a depth between 0.8 m and 1.5 m, and 2% of cavities occurred at a depth more than 1.5 m from the pavement surface. Therefore, 98% of the cavities were distributed within 1.5 m depth, the average depth of underground utilities, and the cavity scale was small and mainly occurred in the shallow layer. Such cavities are likely to expand over time and lead to ground subsidence [1].

Ground subsidence due to cavity can bring about various problems, such as casualties, decrease of the safety of the structures, and indirect social costs. Therefore, ground subsidence should be prevented through the exploration and recovery of the cavity under the pavements [2, 3].

Recently, to avoid affecting the flow of traffic, cavity exploration under the pavement has used the mobile multi-GPR (ground-penetrating radar). The location, depth, and cavity scale can be calculated by obtaining waveform GPR data for the cavity under the pavements. The cavity scale can be calculated by confirming the availability of the cavity from the parabolic cross section based on the theory of cavity waveform analysis. Generally, the horizontal axis of the cavity waveform shows the measurement distance, and the vertical axis shows the depth. Furthermore, the cavity scale is calculated by estimating the scale in each direction through the longitudinal and cross-sectional measurements of the image of the cavity waveforms. However, the cavity scale can

be confirmed accurately only through excavation during the restoration process.

On the other hand, cavity exploration and the calculation of the scale are normally divided into two processes: (1) GPR exploration and (2) endoscopic investigation. The GPR exploration calculates the cavity scale on the longitudinal and cross-sectional directions; then, the endoscopic investigation films the inside of the cavity to confirm its depth and width. Considering the cavity scale (height and width), the thickness of the pavement, and the amount of cracks in the pavement, the results of the primary exploration and secondary investigation allow us to determine the level of danger of the cavity. According to the cavity management guidelines established by the city of Seoul, the dangerousness of the cavity is determined on four levels: emergency, priority, general, and observation. Emergency and priority levels indicate the level of danger that the cavity must be restored immediately, while the general and monitoring levels mean that the cavity may expand to a higher level. Therefore, there should be an exact calculation of the cavity scale to monitor the expansion process of the cavity from the general and observation levels to a more dangerous level. Furthermore, the exact calculation of the cavity scale is also important to determine the costs (e.g., materials and equipment) for the restoration of the cavity, if the cavity is at the emergency or priority levels.

Current methods for the measurement of cavity scales are excavating the cavity directly, which leads to social indirect costs due to traffic control as well as the direct costs associated with the excavation and restoration process. Since a difference occurs between the estimation of the cavity scale obtained through the direct excavation and the cavity scale obtained from the GPR exploration, the reliability of the GPR exploration results is degraded. Therefore, in order to ensure the reliability of the GPR exploration results, it is necessary to enhance the accuracy of the cavity scale calculation based on the GPR exploration.

This study compares the cavity scales obtained from the GPR exploration and the direct excavation of the identified cavity. The first exploration was carried out on the actual roadway, and the second exploration was carried out on the mock-up site to prevent the cavity collapse by placing Styrofoam under the ground. Therefore, the study suggests a GPR exploration method for predicting the actual cavity scales by comparing the GPR exploration results with the identified cavity scales.

2. GPR Exploration and Methods for Cavity Scale Calculation

2.1. Principles of GPR Exploration. The ground-penetrating radar emits electromagnetic waves into the underground and receives the electromagnetic waves reflected from a boundary with different electrical properties (e.g., conductivity and permittivity). This system is widely used to investigate the reserves of the resources in mines, buried structures, and terrane information in geophysics [4–6]. GPR exploration is a method to explore the shallow subjects or structures with high resolution by using the transmission of the electromagnetic waves with frequencies higher than tens of MHz and is commonly used as a nondestructive test for the survey of underground pipes under the pavements, cavities as well as cavity exploration of tunnels [7, 8].

The principles of the GPR exploration are shown in Figure 1. The electromagnetic waves emitted from the transmitter antenna are reflected, bent, diffracted, and recorded as waveforms by the reception antenna. The GPR exploration identifies the size and location of the anomalous object by analyzing the changing patterns of the waveforms according to the characteristics of the anomalous object (e.g., boundary, utilities, cavities, and so on) [9].

The high-frequency bandwidth between 10 MHz and 1 GHz used in the GPR exploration falls under the transmission area in which displacement currents are superior compared to conduction currents, and the behavior of the electromagnetic wave remains under the control of the wave equation. The most interesting behavioral characteristics of the GPR waves in the area of the electromagnetic waves are the attenuation and speed. Under the assumption of flat electromagnetic waves, the attenuation (α, [dB/m]) and the phase constant (β, [rad/m]) of the wave area are shown in equations (1) and (2):

$$\alpha = \frac{\sigma}{2}\frac{\mu}{\varepsilon}, \tag{1}$$

$$\beta = \omega\mu\varepsilon. \tag{2}$$

The symbol σ refers to the electrical conductivity (S/m), ε is the permittivity (F/m), μ is the permeability (H/m), and ω is the frequency. Therefore, as the conductivity of the medium increases and the permittivity decreases, the GPR waves show significant attenuations and become irrelevant to the frequency. However, in areas with a frequency higher than 100 MHz, the attenuation rapidly increases due to relaxation effects, and the depth of investigation of the GPR system that uses a wavelength higher than 100 MHz decreases rapidly.

Under the assumption that the penetration ratio of the rocks that constitute the underground is identical to that within a vacuum ($\mu = \mu_0$), the GPR transmission speed (v, [m/ns]) can be defined as in equation (3). The transmission speed of the GPR wave is not related to the frequency and depends only on the permittivity:

$$v = \frac{c}{\sqrt{\varepsilon\gamma}} = \frac{0.3}{\sqrt{\varepsilon\gamma}}. \tag{3}$$

The minimum size of the object that can be explored is called resolution; it varies according to the soil, and it is half of the length of a single wavelength (λ_l). The base wavelength must increase to increase the resolution. However, when the base wavelength increases and the resolution increases accordingly, the depth of the investigation decreases due to an increase of attenuation. When selecting an antenna, the depth of the investigation should be prioritized over the resolution if there is no information on the depth or permittivity of the object. It should be noted that the speed of the GPR wave is a function of the permittivity,

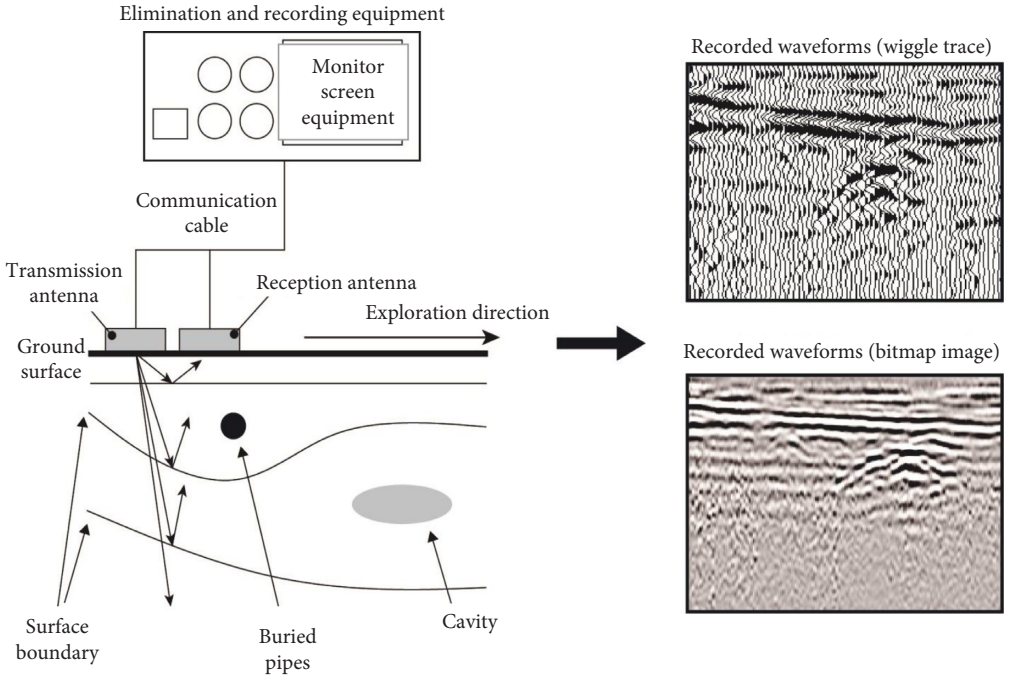

Figure 1: Schematic of the GPR system and waveforms.

and the resolution varies according to the medium. The minimum frequency is decided by the resolution, and the maximum frequency is influenced by the depth of the investigation and the scale of the seismic noise as shown in Table 1.

According to the characteristics of the underground medium, the frequency used for GPR explorations should be appropriately changed according to the stratum of the exploration subject, the status of the surface of the earth, the status of the underground water, and the surrounding environment. When using an antenna with a high base frequency of 500 MHz, the depth of the exploration varies according to the permittivity and the electrical conductivity of the underground, which is generally between 2 m and 3 m. If the surface is an asphalt pavement, the penetration depth is reduced to 1 to 2 m, as the energy of the electromagnetic waves to penetrate to the bottom weakens, reflecting much energy at the boundary of the packaging [10].

GPR reflections transmitted through a pavement structure can determine sublayer electromagnetic properties [11–13]. The electromagnetic property measured more frequently by pavement engineers is the dielectric constant (ε) because it is primarily influenced by soil water content [14]. From the perspective of material engineering, soils are composite material systems comprised of inorganic minerals, organic particles, water, and air. As a result, the dielectric characteristics of the soil are a function of the dielectric constants of the individual soil components, the volume fraction of each component, their geometrics, and the electrochemical interactions between the components [15]. Table 2 summarizes the published dielectric constants of typical pavement soil constituents [14].

When a low-frequency antenna of 100 MHz is used to increase the penetration depth, it is difficult to distinguish the reflective signals from shallow areas due to the interference of the direct waves emitted from the transmission antenna to the reception antenna. Therefore, the electrical characteristics of the underground medium and the frequency used for the exploration should be investigated in advance to ensure the appropriate exploration depths and resolution.

2.2. Analysis of the Cavity Exploration and the Calculation of the Cavity Scale. As shown in Figure 2, the GPR exploration equipment used in this study is mounted on a vehicle. Its base frequency is 400 MHz, and the exploration depth on paved pavements is within 2 m. This is effective in detecting the cavities and underground utilities of 0.15 m or larger within the depth of one meter (0.3 m within 2 m of depth). In addition with the multichannel GPR exploration equipment, there are three-dimensional interpretations, which allow us to detect abnormal signals according to the difference in materials as well as in the permittivity of identical materials.

The GPR exploration equipment consists of GPR antennae, surface image camera, GPS measurement equipment, and positioning cameras, which allow us to identify the exact location of abnormal signals from the surface. In addition, the integrated analysis program of the multichannel GPR and the positioning system increase the reliability of the exploration results.

First, the exploration uses a piece of software that records and controls the exploration data and sets the antenna arrangement, sampling intervals, and initial values of the data locations. The data are obtained by constructing a reception

Table 1: Relationship between the variables of underground electrical characteristics, GPR exploration, and frequency.

Measurement variable	Permittivity			Conductivity			Frequency		
	Low	⟶	High	Low	⟶	High	Low	⟶	High
Velocity of electromagnetic wave	Fast	⟶	Slow		—			—	
Attenuation	High	⟶	Low	Low	⟶	High	Low	⟶	High
Depth of investigation	Shallow	⟶	Deep	Deep	⟶	Shallow	Deep	⟶	Shallow
Wavelength	Long	⟶	Short		—		Long	⟶	Short
Resolution	Low	⟶	High		—		Low	⟶	High

Table 2: Dielectric values of the typical pavement soil and layer constituents.

Constituent	Dielectric value
Air	1
Freshwater	8
Ice	4
Bedrock (granite)	5–7
Clay	25–40
Silt	16–30
Silty sand	7–10
Sand subbase	4–6
Gravel base	4–7
Glacial till	8–18
Asphalt concrete	4–8
Slag asphalt concrete	8–15
Portland cement concrete	8–10
Bitumen bound base	6–7
Cement bound base	8–10

and transmission channel, DMI, and exploration system. Afterwards, the results are analyzed through data processing, such as preprocessing, interpolation, and migration of data, using the analysis programs for exploration data. The sectional data analyses are conducted according to the channels through the integrated management of the positioning system and then comparing and analyzing the abnormal locations with the surface clips, filtering the signals from objects such as underground utilities and manholes.

On the other hand, if the GPR exploration consists of a one-dimensional arrangement and detects cavities or underground pipes, the target is represented as a parabola on the GPR data. Therefore, the system is able to obtain data from detecting the strength of the reception signal and the delay in transmitting and receiving the electromagnetic waves.

As shown in Figure 3, when the GPR sensors shown with red dots are aligned, there is a particular object (cavity or underground pipe) below them, and the GPR sensors transmit and receive individual electromagnetic waves, the delay becomes longer as the sensor is further away from the target object; as the distance increases, the strength of the signal reflected back is weakened. If this is represented in a two-dimensional space with time axis and sensor arrangement direction, it assumes a parabolic shape. The parabola has a gradual slope for materials with low permittivity and has a steeper slope for materials with high permittivity [16]. The slope waveform has a parabolic shape, and the major type of waveform is shown in Figure 4.

Figure 5 shows a method to differentiate the cavity according to the white and black parts of the waveform, based on the fact that air and medium have different permittivities. It shows a reflected form in the case of homogeneous medium and cavity. In the case of a homogeneous medium without cavity under the pavement, depending on the direction of the depths, the relative permittivity increases and the phase switches from black to white. When there are cavities under the pavements, the permittivity decreases in the direction of the depth, reversing the phase of the reflecting waves by 180 degrees and switching the phase from white to black [17–19].

In the results of the cavity explorations, the horizontal axis and the vertical axis represent the distance and depth, respectively, and the exploration results are interpreted as the reflection patterns shown in the cross-section planes. In the clip of the results of the planes, the color shows the strength of the electromagnetic waves that are transmitted and allows us to distinguish between cavities and underground pipes according to the characteristics of the trace waveforms. However, although the depth of the explored abnormal object is determined by the continuous observation of the electromagnetic waves and the permittivity constant of the medium, there may be errors as it is difficult to determine accurately the permittivity constant according to the medium.

The abnormal signals from the clips of the planes should be selected first to analyze the signal of the cavity. There are patterns of straight lines in the case of underground pipe; however, a pattern formed in a particular area along the boundary that shows an extreme change in amplitude is considered a cavity, and the cavity is determined by the combination of the plane, longitudinal, and cross sections. As mentioned previously, the signals for the cavity through the clips of the longitudinal sections are shown in a parabolic shape; the depths are identified through the distance between the apical area, where large changes begin; finally, the surface and the longitudinal lengths are identified through the width of each end of the parabola. Generally, the longitudinal and cross-sectional widths of the cavity waveforms are calculated in the range between 60 and 100% of each end, but when it is needed, migration is first conducted, which is followed by the analysis of the reflection states. Using these methods, the examples of calculation based on the width of each end of the parabola from the cavity waveforms obtained from GPR exploration are shown in Figure 6.

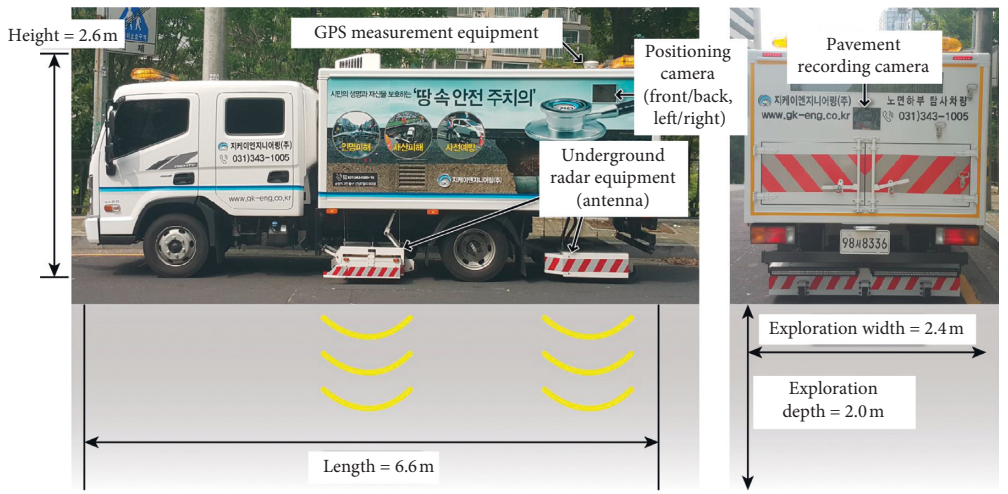

Figure 2: Extended multichannel GPR exploration equipment mounted on a vehicle.

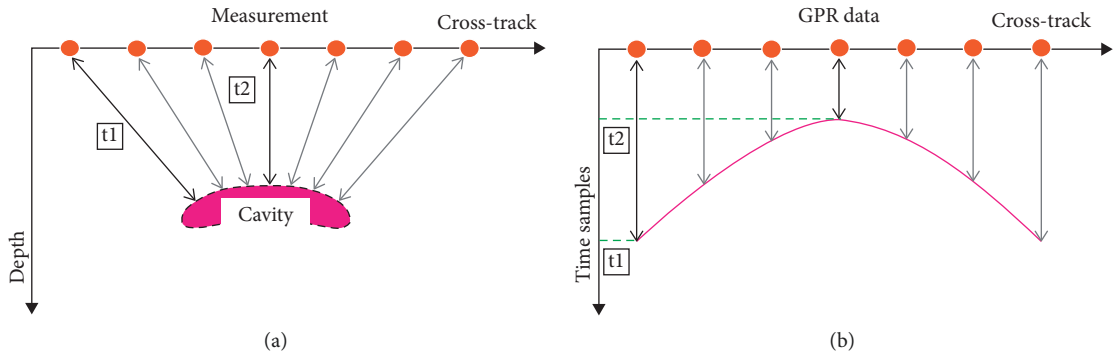

Figure 3: Parabolic signature in the GPR Data. (a) GPR detection. (b) Parabola projection of GPR data.

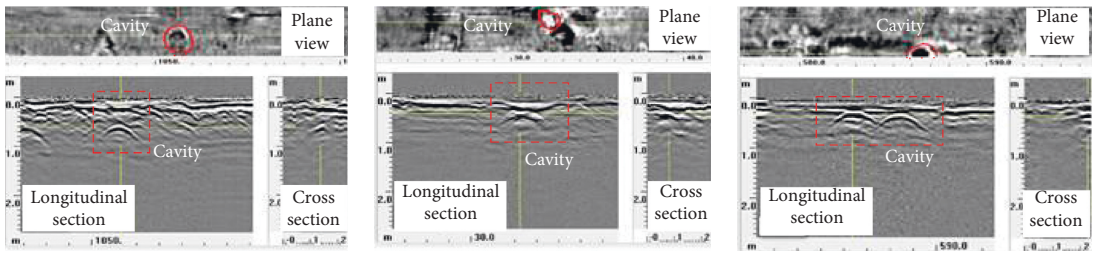

Figure 4: Common types of cavity waveforms. (a) Wedge type. (b) Box type. (c) Continuous type.

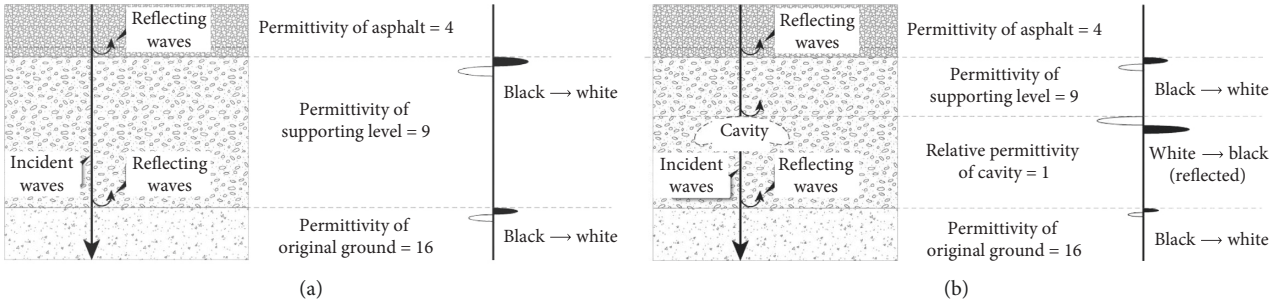

Figure 5: Reflected status of the polarity of the reflected wave. (a) In medium of homogeneous typical strata. (b) In cavity.

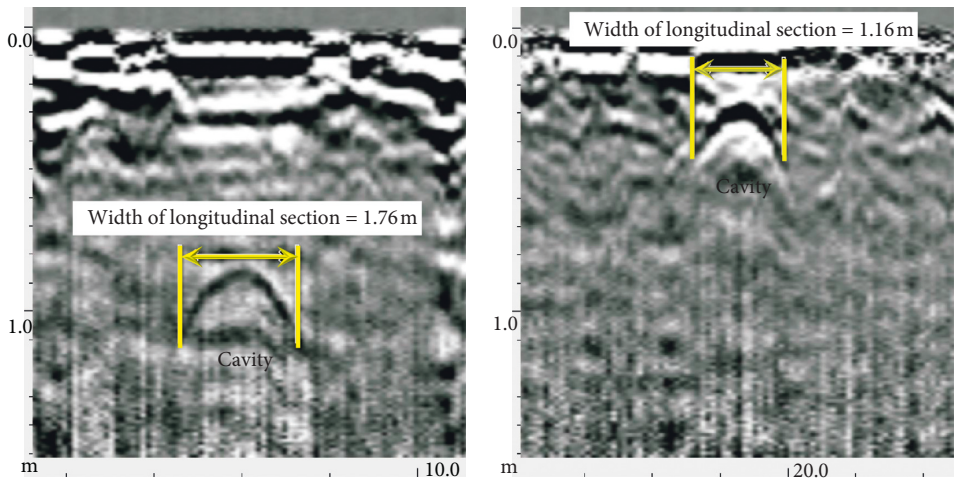

Figure 6: Measurement example of scale (soil depth and width) by the cavity waveforms. (a) Depth: 0.9 m and width: 1.0 m. (b) Depth: 0.3 m and width: 0.5 m.

3. A Comparison of Evaluation Results on the Cavity Scale

3.1. Evaluation Methods. The calculation of the cavity scales according to the GPR waveforms is extremely important to evaluate the danger levels for managing the cavity. The cavity scales are calculated at a set ratio by considering the permittivity of the medium under the pavements, based on the total width of the lower parabola of the cavity waveform obtained from the longitudinal section and the cross section.

Therefore, in this study, we compared the cavity scales calculated on the basis of the exploration of the cavity with those identified through direct excavation. To evaluate the calculation results of the cavity scales through GPR exploration, the soil depth on the top of the cavity and the cavity scale were compared for 10 cavities in three regions. Based on the results, the relationships between the predicted cavity and the identified cavity were analyzed.

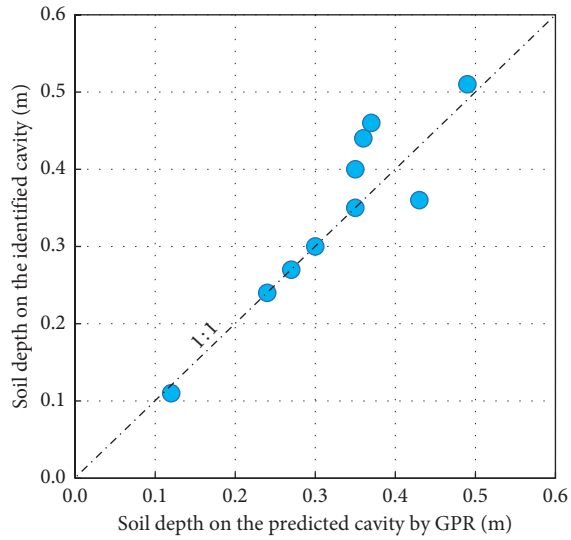

Figure 7: Relationship of the soil depth on the predicted cavity and the identified cavity.

3.2. Evaluation Results. Figure 7 illustrates the relationship between the depths of the predicted cavity and the identified cavity. The ratio of the identified soil depth and the predicted soil depth was analyzed in order to evaluate the error bound of the soil depth on the cavity. The result showed that the difference between the identified soil depth and the predicted soil depth was about 12% to 19%, when the identified soil depth was more than 0.4 m. This result means that the GPR exploration depth is limited. Although some data have differences, the relationship between the identified soil depth and the predicted soil depth is close to 1 : 1 gradient. Therefore, it was confirmed that the predicted soil depth from the pavement layer was approximately the same as the identified soil depth.

Table 3 and Figure 8 show the results of the analysis of the relationship between the soil depths of the identified cavity, the soil depth of the predicted cavity according to the GPR waveforms, and the total width (longitudinal and cross-sectional widths). As shown in Table 3, the soil depth of the identified cavity was from 0.11 m to 0.51 m, and the soil depth was divided into three ranges based on the depth relationship (see Figure 8) between the locations of the predicted cavity and the identified cavity. As a result of calculating the arithmetic mean of the soil depth by the range of the identified cavity, the mean soil depths of each range were 0.23 m, 0.37 m, and 0.47 m, respectively. Based on these results, the minimum, maximum, and the mean of the predicted cavity according to soil depths were compared. The results showed that, as the soil depth decreased, the soil depths of the predicted cavity and the identified cavity were almost identical, and this is identical to the qualitative results shown in Figure 7. Furthermore, as the soil depth increased, the differences in the longitudinal width of the predicted cavity increased; however, the differences in the cross-section width were similar.

Table 3: Calculation results of mean difference in the scale of the predicted cavity according to the soil depth of the identified cavity.

Average soil depth of the identified cavity [soil depth range] (m)	Difference in soil depth (m)			Difference in longitudinal section (m)			Difference in cross section (m)		
	Minimum	Maximum	Mean	Minimum	Maximum	Mean	Minimum	Maximum	Mean
0.23 [0.11~0.30]	−0.07	0.01	−0.02	0.00	0.35	0.17	0.00	0.40	0.25
0.37 [0.35~0.40]	−0.05	0.00	−0.02	0.10	0.30	0.20	0.10	0.60	0.28
0.47 [0.44~0.51]	−0.09	−0.02	−0.06	0.20	0.60	0.40	0.20	0.40	0.28

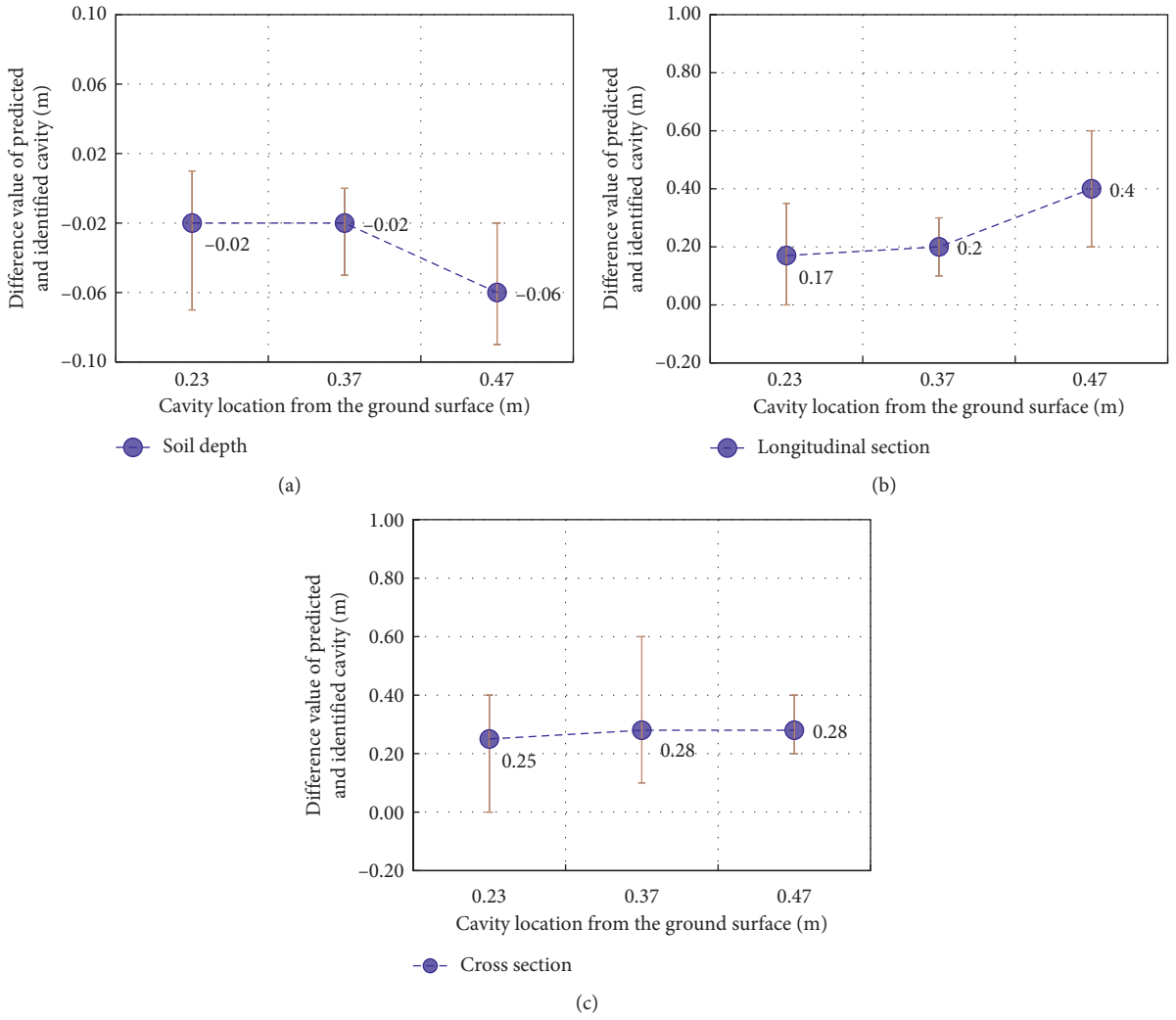

Figure 8: Difference between the predicted cavity scale and the identified cavity scale according to the location of the cavity. (a) Soil depth. (b) Longitudinal section. (c) Cross section.

The difference in the widths of the predicted cavity and the identified cavity as well as the scale ratios were calculated for the longitudinal and cross sections to compare the cavity scales of the predicted cavity and the identified cavity, as shown in Table 4. First, according to the soil depth of the location of the cavity, the differences in the widths of the predicted cavity and the longitudinal and cross sections of the identified cavity were compared. As a result, it was generally difficult to confirm a specific tendency for the difference in scales of the identified and the predicted cavity in longitudinal and cross sections according to the soil depth at the top of the cavity, as shown in Figure 9. This may be due to irregular differences in scales because of some collapses of the soil around the cavity due to external drilling along with the errors of the analysis. Therefore, we concluded that there was no significant relationship between the scales of the identified cavity and the predicted cavity, according to the soil depth of the cavity. In addition, we also analyzed the ratio of the total width of the GPR waveforms in a parabolic form and the scales of the identified cavity (scales of identified cavity ($C_{identified}$)/scales of predicted cavity ($C_{predicted}$)). As shown in Figure 10, the ratio of the scales of

Table 4: Calculation results of the difference in scales between the predicted cavity and the identified cavity according to the soil depth.

Analyzed cavities	Soil depth (m)	Identified cavity (m)		Difference of predicted and identified values (m)		$C_{identified}/C_{predicted}$ (%)	
		Longitudinal section	Cross section	Longitudinal section	Cross section	Longitudinal section	Cross section
Cavity 1	0.11	1.00	0.90	0.30	0.30	76.9	75.0
Cavity 2	0.24	0.50	0.40	0.35	0.40	58.8	50.0
Cavity 3	0.27	1.50	1.20	0.00	0.00	100.0	100.0
Cavity 4	0.30	1.60	0.50	0.00	0.30	100.0	62.5
Cavity 5	0.35	1.00	0.50	0.30	0.10	76.9	83.3
Cavity 6	0.36	1.60	2.10	0.10	0.60	94.1	77.8
Cavity 7	0.40	1.20	0.65	0.20	0.15	85.7	81.3
Cavity 8	0.44	0.70	1.40	0.60	0.20	53.8	87.5
Cavity 9	0.46	1.80	0.40	0.20	0.40	90.0	50.0
Cavity 10	0.51	1.00	0.95	0.40	0.25	71.4	79.2

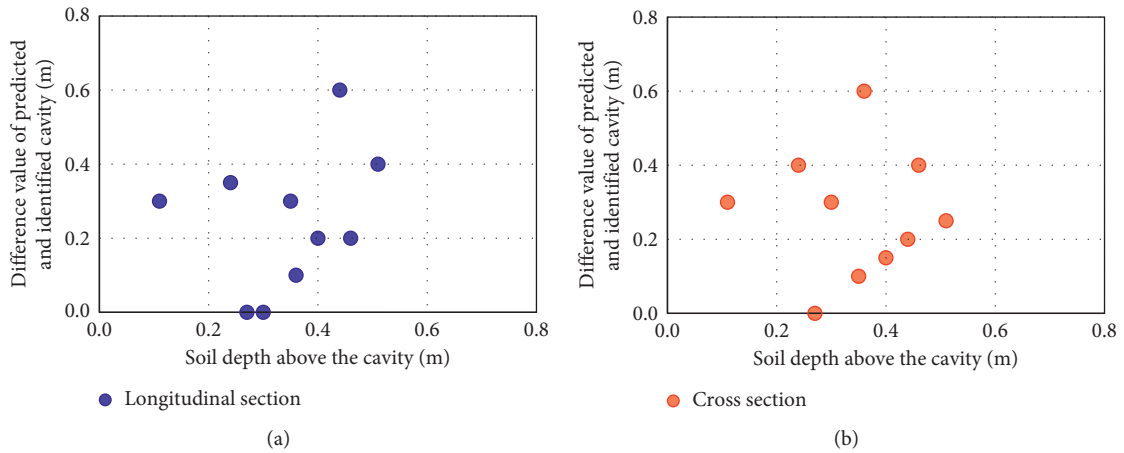

Figure 9: Relationship between the differences in cavity scales according to the soil depth. (a) Longitudinal section. (b) Cross section.

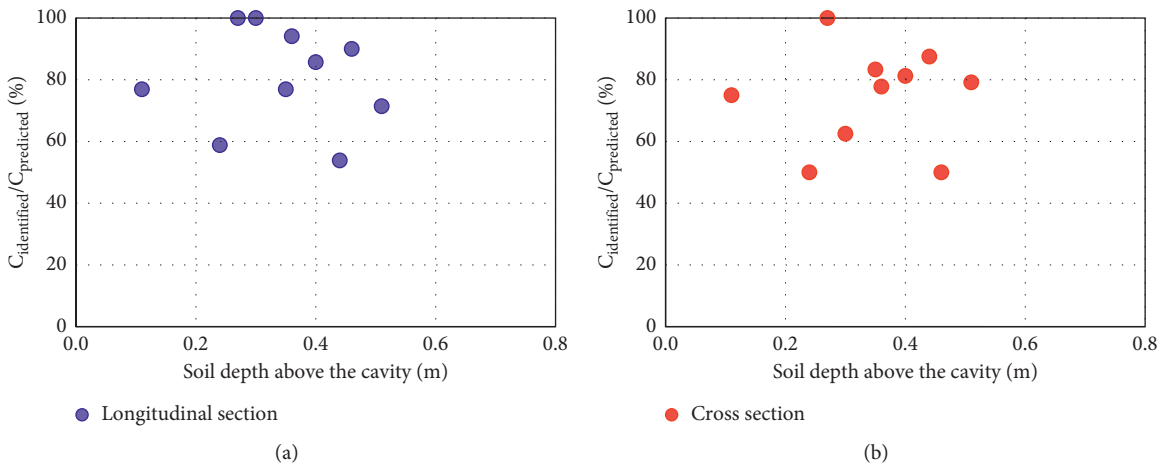

Figure 10: Relationship of the cavity scale ratio according to the soil depth. (a) Longitudinal section. (b) Cross section.

the identified cavity to the total width of the predicted cavity was between 53.8% and 100% for the longitudinal sections and between 50% and 100% for the cross sections. In other words, it is estimated that the cavity explored through GPR was larger compared to the actual cavity.

Although the soil depths on the top of the predicted cavity and the identified cavity were similar, there were no strict tendencies for the differences and the ratios of the cavity scales. The reason may be the collapses and sinks of some cavities during the examination process, and so, the

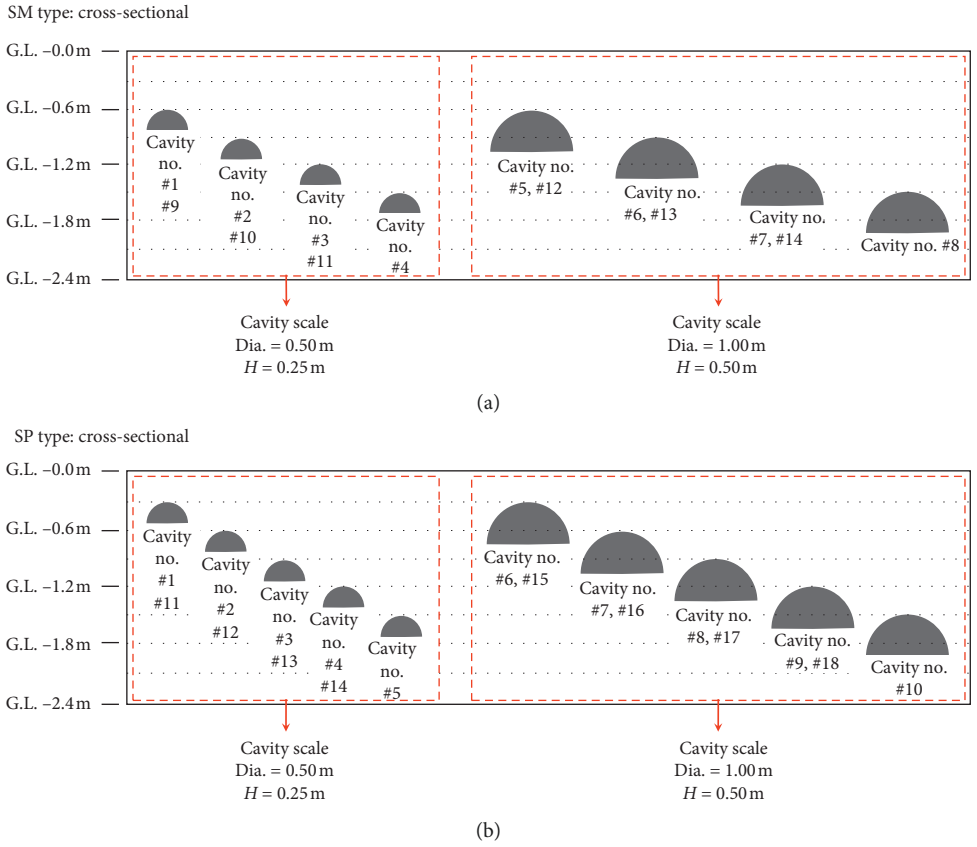

Figure 11: Experiment types. (a) Detailed map of SM type. (b) Detailed map of SP type.

study suggested a calculation method of the cavity scale through a test-bed experiment that artificially structuralizes mock-up cavities.

4. Evaluation of the Cavity Scale Based on a Test-Bed Experiment

Although the relationship between the predicted and identified cavity scales was evaluated based on the field data, it was difficult to derive a clear correlation. Therefore, this study attempted to compare the cavity scales through the ratio and difference of the predicted and the identified cavities based on a mock-up test and attempted to suggest a calculation method for cavity scales.

4.1. Construction of the Mock-Up Cavities and the Experimental Methods. In the test-bed experiment, the mock-up cavities were constructed in 32 locations considering the on-site condition according to the depth and the scale of the cavity. The mock-up cavity used Styrofoam in a hemispherical structure with 0.5 m and one meter in diameter and 0.25 m and 0.5 m in height and was planted in the ground. The reason for using Styrofoam was that a previous study showed that the permittivity constant of Styrofoam is similar to that of air [20]. The vertical locations of the mock-up cavities were 0.3 m, 0.6 m, 0.9 m, 1.2 m, and 1.5 m from the ground surface, and the space between each cavity was 0.3 m.

After excavating the ground, Styrofoam was placed in the planned locations, which were then covered in backfill soil. For the backfill soil of the top of the mock-up cavities, we used SM (silty sand) and SP (sand mixed with silt), which are commonly used in Korea as backfill soils. The GPR explorations used the same equipment as described for the previous experiment.

The purpose of this experiment was to suggest a method to quantitatively estimate the cavity scale through a comparison between the predicted cavity and the identified cavity. Therefore, there must be an excavation of cavity that can be clearly compared to the mock-up cavities. However, after simulating the mock-up cavities, it was found to be difficult to obtain clear GPR exploration results due to the collapses of some cavities and the irregular pavement surface of the unpaved pavements. Hence, we used the test results of 10 cases only that were relatively clear and, thus, comparable with the mock-up cavities. The summary of the experiment types is shown in Figure 11.

4.2. Results and Discussion. Table 5 shows the soil depth and the longitudinal and cross sections of the predicted cavity (GPR exploration results) and the identified cavity (mock-up cavities) according to the soil types. The soil depths of the predicted cavity and the identified cavity were approximately −0.06 m to 0.04 m, which were similar. This is similar to the results of experiments on cavities on the roadway. However, the difference in the longitudinal width of the

Table 5: Calculation results of the difference in soil depths and scales between the predicted cavity and the identified cavity.

Type	Cavity no.	Soil depth (m)			Longitudinal section (m)			Cross section (m)		
		Predicted cavity	Identified cavity	Difference	Predicted cavity	Identified cavity	Difference	Predicted cavity	Identified cavity	Difference
SM	#5	0.63	0.60	0.03	1.45	1.00	0.45	1.50	1.00	0.50
	#12	0.54	0.60	−0.06	1.53	1.00	0.53	1.50	1.00	0.50
	#13	0.84	0.90	−0.06	1.76	1.00	0.76	1.80	1.00	0.80
SP	#1	0.26	0.30	−0.04	0.83	0.50	0.33	0.80	0.50	0.30
	#11	0.32	0.30	0.02	0.86	0.50	0.36	0.90	0.50	0.40
	#6	0.32	0.30	0.02	1.30	1.00	0.30	1.30	1.00	0.30
	#15	0.28	0.30	−0.02	1.22	1.00	0.22	1.30	1.00	0.30
	#2	0.54	0.60	−0.06	1.03	0.50	0.53	1.10	0.50	0.60
	#7	0.64	0.60	0.04	1.59	1.00	0.59	1.60	1.00	0.60
	#16	0.59	0.60	−0.01	1.52	1.00	0.52	1.50	1.00	0.50

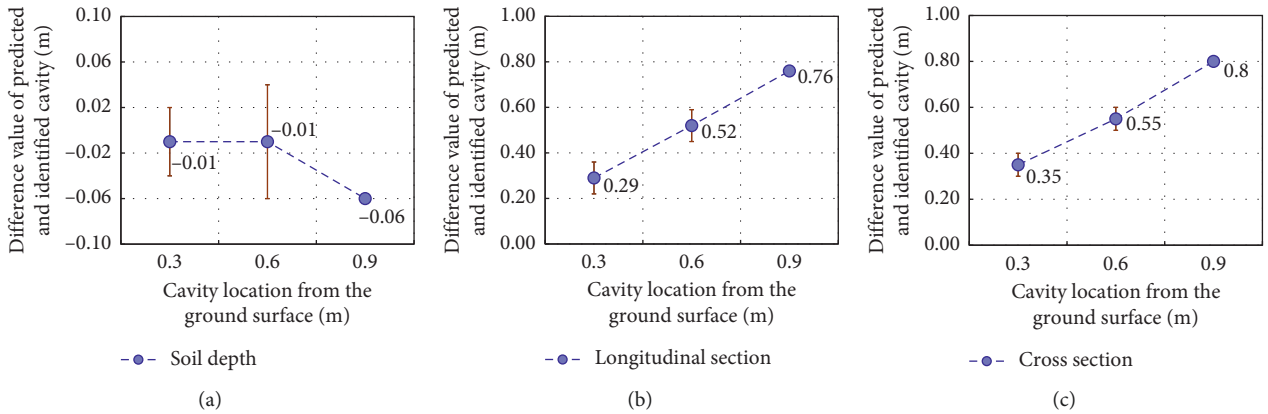

Figure 12: Difference between the predicted cavity scale and the identified cavity scale according to the location of the cavity. (a) Soil depth. (b) Longitudinal section. (c) Cross section.

predicted cavity and the identified cavity was found to be 0.22 m to 0.76 m depending on the depth of the cavity, and the difference in cross-sectional width was found to be 0.30 m to 0.80 m.

Figure 12 shows the results of the correlation analysis using the mean differences between the predicted cavity and the identified cavity concerning the soil depth, longitudinal sections, and cross sections when the buried depths were at 0.3 m, 0.6 m, and 0.9 m, respectively. The results show that when the soil depths were at 0.3 m and 0.6 m, there were not many differences in the vertical location of the predicted cavity and the identified cavity, but as the soil depth increased, the difference increased as well. This is also similar to the tendency shown in the experiment on cavities on the roadway. However, as the soil depth increases, the differences in the longitudinal and cross sections of the predicted cavity and the identified cavity continuously increased. Based on these results, we were able to show that, as the depth of the cavity (soil depth) increases, the scales of longitudinal and cross sections of the predicted cavity were larger than those of the identified cavity.

Table 6 shows the scale ratio of the predicted cavity and the identified cavity according to the conditions of the experiment. The scale ratio was determined as the ratio of the identified cavity to the predicted cavity on the soil depth, longitudinal width, and cross-sectional width. The results showed that the scale ratio of soil depth was 94% to 111%, and the scale ratios of the longitudinal and cross sections were 49% to 82% and 45% to 77%, respectively. There was a small difference in the scale ratio of soil depth between the predicted cavity and the identified cavity, but the scale ratio of the longitudinal and cross-sectional width was large. This shows that the cavity scales predicted by GPR explorations are larger than the actual cavities for the scale ratios of the longitudinal and cross sections. Although the scale of soil depth predicted by the GPR exploration is relatively reliable, there is a possibility that the exploration results for the longitudinal and cross-sectional width reveal large errors.

On the other hand, soil types did not show particular relationships with buried depth, cavity scale, and scale ratio. This is because there are no large differences in permittivity according to the types of SM and SP, as suggested by Saarenketo [21].

4.3. Suggestions of Evaluation Method for Prediction of the Cavity Scale. It is extremely difficult to estimate the scale of a cavity in the ground accurately. Based on the results of the mock-up test, we found no relationship between the cavity scale and the soil type. However, it was found that the GPR

Table 6: Calculation results of the scale ratio.

Soil type	Cavity no.	Soil depth (m)	Cavity scale (longitudinal section = cross section) (m)	Cavity height (m)	Scale ratio (identified cavity/predicted Cavity)		
					Soil depth (%)	Longitudinal section (%)	Cross section (%)
SM	#5	0.6	1.0	0.5	95	69	67
	#12	0.6			111	65	67
	#13	0.9			107	57	56
SP	#1	0.3	0.5	0.25	115	60	63
	#11	0.3			94	58	56
	#6	0.3	1.0	0.5	94	77	77
	#15	0.3			107	82	77
	#2	0.6	0.5	0.25	111	49	45
	#7	0.6	1.0	0.5	94	63	63
	#16	0.6			102	66	67

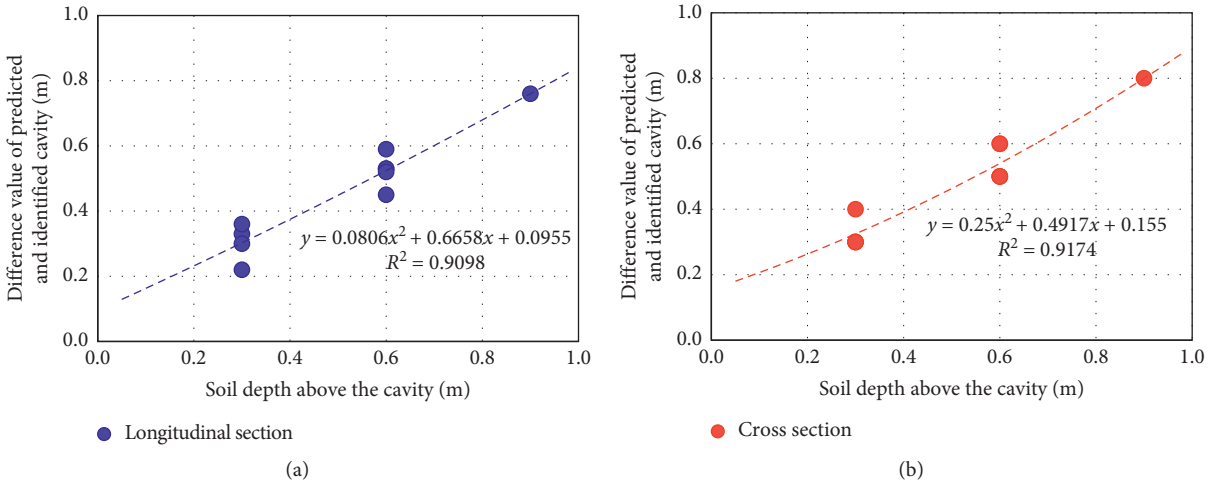

Figure 13: Correlation of the cavity scale according to the soil depth. (a) Longitudinal section. (b) Cross section.

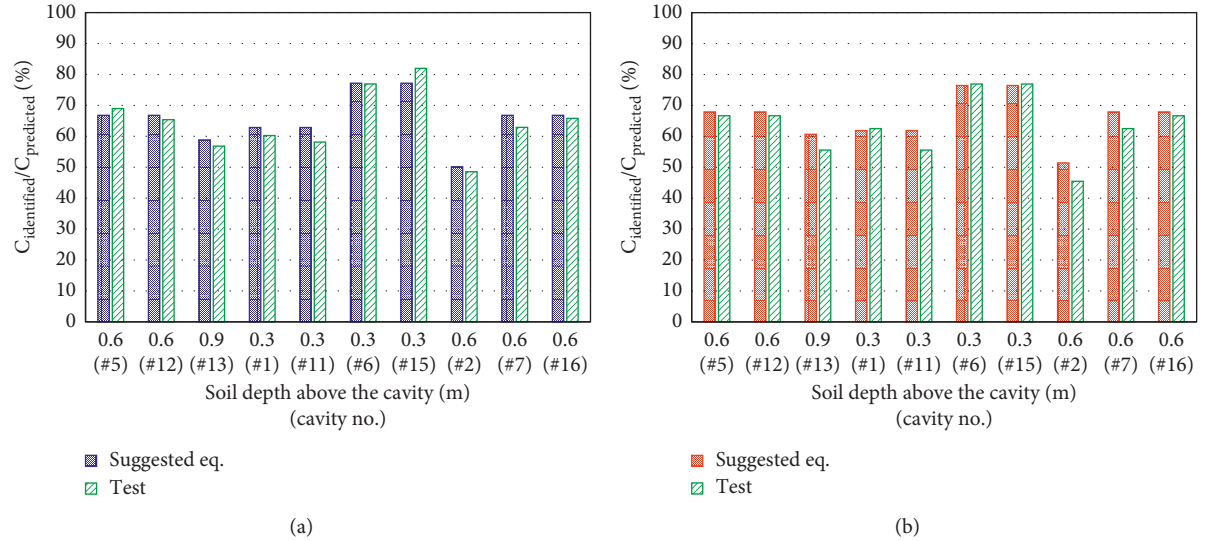

Figure 14: Evaluation results by the applied evaluation method. (a) Longitudinal section. (b) Cross section.

exploration results were relatively accurate in estimating the depth of the cavity (soil depth). In addition, as the soil depth increases on top of the cavity, the plane scales of the cavity (longitudinal and cross sections) are predicted to be larger than the actual scales. Therefore, based on the relationship between the structuralized mock-up cavity (identified

cavity) scale and the predicted cavity scale by the results of GPR exploration (see Table 5), we suggest a formula to estimate the cavity scale using the differences (predicted cavity minus identified cavity) in the longitudinal and cross sections, according to the soil depth as shown in Figure 13. Considering the nonlinear increasing trend of the difference of the plane scale of the cavity in the experimental cases according to the increase of the soil depth, the formula was determined as a second-order polynomial.

We compared the scale ratio of the cavity predicted from the mock-up test and the scale ratio calculated with the proposed formula as shown in Figure 14. The scale ratio obtained by applying the formula was generally larger than the scale ratio obtained from the results of the experiment. In particular, the increase rate was larger for the cross sections, where the differences in scale were relatively large in comparison to the longitudinal scale. Therefore, it is possible to quantitatively estimate the cavity scale based on the calculation method suggested in this study. However, the formula should be applied to more cavity data to enhance its reliability.

5. Conclusions

In this study, the GPR exploration method was carried out on both actual roadway and mock-up site to compensate for the problems caused by excavation and restoration process. An empirical GPR exploration method for predicting the actual cavity scales by comparing the GPR exploration results with the identified cavity scales was suggested. The results are summarized as follows:

(1) This study compared the cavity scales obtained from GPR exploration results and the direct excavation of the identified cavity. It was confirmed that the predicted soil depth by GPR exploration was similar to the identified soil depth, but the predicted cavity scale by GPR exploration overestimated the longitudinal and cross-sectional widths compared to the identified cavity scale.

(2) In the experiment on the actual roadway, there was no clear trend for the differences and the ratios of the cavity scales between GPR exploration results and identified cavity. The reason is assumed to be the collapse of cavity during the examination process. Thus, an additional mock-up test was performed to prevent the cavity collapse by placing Styrofoam under the ground. Although the soil depth of the predicted cavity and the identified cavity was similar, the difference in the longitudinal and cross-sectional widths increased as the soil depth increased. Therefore, cavity scales predicted by GPR explorations were larger than the actual cavities for the scale ratios of the longitudinal and cross sections.

(3) Based on the correlation between the predicted cavity scales by GPR exploration and the cavity scales identified in the mock-up test, it is possible to qualitatively estimate the cavity scales using the empirical formula proposed in this study.

Data Availability

The data used to support the findings of this study are available from the corresponding author upon request.

Conflicts of Interest

The authors declare that they have no conflicts of interest.

Acknowledgments

This work was supported by Korea Environment Industry & Technology Institute (KEITI) through Public Technology Program based on Environmental Policy Project, funded by the Korea Ministry of Environment (MOE) (no. 2016000700001).

References

[1] *A Study on the Mechanisms of Pavement Subsurface Cavity and its Management Plans*, in Korean, Seoul City, South Korea, 2016, in Korean.

[2] J. J. Park, H. S. Shin, Y. Chung, S. K. You, and G. Hong, "A study on the open cut restoration of underground cavity using concrete mat," *Journal of Korean Geosynthetics Society*, vol. 18, no. 1, pp. 55–65, 2019.

[3] H. Y. Chae, "Study on subsurface collapse of pavement surface and cavity search in urban area," *Tunnel & Underground Space*, vol. 27, no. 6, pp. 387–392, 2017.

[4] D. J. Daniels, "Ground penetrating radar," in *Encyclopedia of RF and Microwave Engineering*, John Willy & Sons, Inc., Hoboken, NJ, USA, 2005.

[5] N. J. Cassidy, R. Eddies, and S. Dods, "Void detection beneath reinforced concrete sections: the practical application of ground penetrating radar and ultrasonic techniques," *Journal of Applied Geophysics*, vol. 74, no. 4, pp. 263–276, 2011.

[6] Y. V. Kang and H. Hsu, "Application of ground penetrating radar to identify shallow cavities in a coastal dyke," *Journal of Applied Science and Engineering*, vol. 16, no. 1, pp. 23–28, 2013.

[7] Korean Society of Earth and Exploration Geophysicists, *Practical Guidelines for Geophysical Exploration*, Korean Society of Earth and Exploration Geophysicists, Daejeon, South Korea, 2011, in Korean.

[8] Y. S. Han, "Numerical analysis and exploring of ground condition during groundwater drawdown environment in open-cut type excavation," *Journal of the Korean Geotechnical Society*, vol. 34, no. 11, pp. 93–105, 2018.

[9] A. Arisona, M. Nawawi, K. S. Ishola, and L. O. Safiuddin, "Forward modeling of ground penetration radar for the reconstruction of models response profiles using synthetic data," *Journal of Geology & Geophysics*, vol. 6, no. 3, p. 3, 2017.

[10] C. Berthelot, D. Podborochynski, T. Saarenketo, B. Marjerison, and C. Prang, "Ground-penetrating radar evaluation of moisture and frost across typical saskatchewan pavement soils," *Advances in Civil Engineering*, vol. 2010, Article ID 416190, 9 pages, 2010.

[11] K. Grote, S. Hubbard, and Y. Rubin, "GPR monitoring of volumetric water content in soils applied to highway construction and maintenance," *The Leading Edge*, vol. 21, no. 5, pp. 482–504, 2002.

[12] K. Grote, S. Hubbard, J. Harvey, and Y. Rubin, "Evaluation of infiltration in layered pavements using surface GPR reflection

techniques," *Journal of Applied Geophysics*, vol. 57, no. 2, pp. 129–153, 2005.

[13] A. Benedetto and S. Pensa, "Indirect diagnosis of pavement structural damages using surface GPR reflection techniques," *Journal of Applied Geophysics*, vol. 62, no. 2, pp. 107–123, 2007.

[14] T. Saarenketo and T. Scullion, "Ground penetrating radar applications on roads and highways," Tech. Rep. 1923-2F, Texas Transportation Institute, College Station, TX, USA, 1994.

[15] M. D. Knoll and R. Knight, "Relationships between dielectric and hydrogeologic properties of sand-clay mixtures," in *Proceedings of the 5th International Conference on Ground Penetration Radar*, pp. 45–61, Englewood, CO, USA, 1994.

[16] H. Kong, S. Kim, M. Kim, and S. Han, "A preprocessing method for ground penetrating radar based land-mine detection system," *Journal of the Institute of Electronics and Information Engineers*, vol. 50, no. 4, pp. 931–941, 2012.

[17] I. L. Al-Qadi, S. Lahouar, and A. Loulizi, "GPR: From the state-of-the-art to the state-of-the-practice," in *Proceedings of the International Symposium of Non-destructive Testing in Civil Engineering*, Berlin, Germany, September 2003.

[18] L. B. Conyers, "Analysis and interpretation of GPR datasets for integrated archaeological mapping," *Near Surface Geophysics*, vol. 13, no. 6, pp. 645–651, 2015.

[19] A. P. Annan, "11. Ground-penetrating radar," *Near-Surface Geophysics*, vol. 13, pp. 357–438, 2005.

[20] I. L. Al-Qadi, Z. Leng, S. Lahouar, and J. Baek, "In-place hot-mix asphalt density estimation using ground-penetrating radar", *Transportation Research Record: Journal of the Transportation Research Board*, vol. 2152, no. 1, pp. 19–27, 2010.

[21] T. Saarenketo, *Electrical properties of road materials and subgrade soils and the use of ground penetrating radar in traffic infrastructure surveys*, Ph.D. thesis, University of Oulu, Oulu, Finland, 2006.